electronics

MDPI

Essay

Research on Adaptive Fuzzy Fractional-Order Backstepping Control of Magnetic Levitation Linear Synchronous Motors

Yunpeng Sun [1,*], Tao Fang [1], Yu Zhang [2], Wanning Bai [1] and Letong Xu [1]

[1] School of Electrical Engineering, Shenyang Institute of Engineering, Shenyang 110136, China; 12025101110@stu.sie.edu.cn (T.F.); 12025101301@stu.sie.edu.cn (W.B.); 12025101418@stu.sie.edu.cn (L.X.)
[2] Panshan County Power Supply Company, State Grid Liaoning Panjin Power Supply Company, Panjin 124114, China; zhangyu411521@163.com
* Correspondence: sunyp@sie.edu.cn; Tel.: +86-150-0408-0138

Abstract

For the magnetic levitation platform linear synchronous motor suspension system, an adaptive fuzzy fractional-order backstepping control method is designed to enhance system performance. Based on an analysis of the operational mechanism of the magnetic levitation linear synchronous motor (MLLSM) suspension system, its mathematical model and state-space equations are derived. In order to cope with the pronounced nonlinearity exhibited by the MLLSM suspension system, nonlinear coordinate mapping is employed to perform input–output feedback linearization. In order to improve the convergence speed and control accuracy of the system, fractional-order theory is applied to design a fractional-order virtual stability function. This paper designs a fractional-order backstepping controller, and a fuzzy system is employed to approximate the uncertain unknown functions in the MLLSM levitation system. A Lyapunov function is constructed to prove system stability. Experimental results indicate that the adaptive fuzzy fractional-order backstepping control improves the dynamic response of the levitation system and effectively attenuates uncertain disturbances.

Keywords: magnetic levitation platform; linear synchronous motor; fractional-order backstepping control; fuzzy system

1. Introduction

Compared to traditional linear CNC machines, magnetic levitation linear synchronous motors (MLLSM) can achieve stable platform suspension by controlling the suspension system [1–3], fundamentally eliminating the impact of friction on the system, reducing system losses, and improving reliability. However, the elimination of intermediate components means that external disturbances and other uncertain factors directly affect the MLLSM suspension system, significantly increasing the system's control complexity. Therefore, the control system design must suppress these uncertain factors to meet high-precision requirements.

Since backstepping control (BC) can achieve good global tracking performance, it is widely used in the control of suspension systems [4–6]. However, backstepping control requires high accuracy of the system dynamic model, and uncertainties such as external disturbances and sudden load changes can affect the control performance. Reference [7] designed a robust integral backstepping controller, significantly reducing overshoot, convergence time, and steady-state error. Reference [8] presented an adaptive control strategy that integrates command filtering, backstepping, and sliding mode control to achieve finite-time

Check for updates

Academic Editor: Kan Akatsu

Received: 2 September 2026
Revised: 20 October 2026
Accepted: 22 October 2026
Published: 28 October 2026

Copyright: © 2026 by the authors. Licensee MDPI, Basel, Switzerland. This article is an open access article distributed under the terms and conditions of the Creative Commons Attribution (CC BY) license.

trajectory tracking under bounded model uncertainties and external disturbances. Reference [9] proposed an adaptive backstepping control capable of adapting to varying payloads while maintaining performance. Reference [10] presented a fuzzy adaptive output-feedback control scheme that achieves finite-time stability by employing a fuzzy logic system to estimate unknown nonlinear functions in the model. Reference [11] presented a control method that combines fuzzy systems, fuzzy neural networks, and backstepping to guarantee the accuracy, stability, and efficiency of the control system. Reference [12] presents an adaptive backstepping control scheme (ABC) designed for levitation systems to improve the system's position tracking performance. Reference [13] integrates the merits of adaptive backstepping control (ABC) and sliding mode control (SMC) to develop a hybrid adaptive backstepping sliding mode control (ABSMC) algorithm, which attenuates the effects of uncertain disturbances and enhances the disturbance rejection capability of the levitation system. Reference [14] proposes an adaptive backstepping control strategy that employs a recurrent neural network to solve the position tracking problem of levitation systems, thereby further improving the control accuracy and response speed. Reference [15] utilizes an interval-type fuzzy neural network to handle uncertainties in adaptive backstepping control (ABC), ensuring system stability and rapid dynamic response. Compared to traditional integer-order (IO) controllers, fractional-order (FO) controllers provide the system with higher parameter flexibility, effectively improving both transient and steady-state responses. Reference [16] employs adaptive backstepping neural network control, which can specify the steady-state tracking error bound and simultaneously ensure the global uniform ultimate boundedness of the closed-loop system. Reference [17] applies a fractional-order PID controller to regulate the suspended object in a levitation system, thereby achieving a fast dynamic response. Reference [18] constructs a novel fractional-order integral sliding surface and designs a fractional-order sliding mode controller, further improving the system's control performance. Reference [19] applies fractional-order backstepping control (FOBC) to nonlinear systems and validates the controller's effectiveness through simulation. As fractional-order backstepping control theory continues to develop, fractional-order control has also been adopted in AC servo systems, including linear synchronous motors [20].

In practical applications, uncertainty is often difficult to predict in advance. Therefore, many studies have combined neural networks, fuzzy control, and other methods with sliding mode control to estimate the uncertain factors present in a system. Reference [21] presents an adaptive backstepping complementary sliding mode controller that utilizes a disturbance observer to mitigate the effects of uncertain disturbances on control accuracy, thereby enhancing the system's robustness. Reference [22] designs an adaptive law using Lyapunov's theorem to adjust the system control parameters, proposes an adaptive fuzzy backstepping control strategy, and verifies through simulation that this method can effectively enhance the control accuracy of the levitation system, providing a solution to the disturbance suppression problem.

In high-performance motor drives, uncertainty is also handled by online parameter identification and parameter rectification. Instead of approximating an unknown function, these methods estimate explicit physical parameters and correct the model or the controller accordingly. For SPMSM drives, an alternating dual Adaline observer network has identified stator resistance and rotor flux linkage online without signal injection, avoiding rank deficiency under insufficient excitation and counteracting inverter nonlinearity [23]. In predictive control, online model parameter rectification has compensated inductance and flux-linkage errors so that prediction accuracy is preserved under parameter variation [24]. Such methods are effective when the uncertainty is parametric, the model structure is reliable, and the parameters are observable. In the MLLSM levitation subsystem, however, the uncertainty remaining after feedback linearization is a heterogeneous residual of unmod-

eled nonlinearity, armature attraction and external disturbance; it cannot be reduced to a small identifiable parameter set, and these effects enter the same scalar channel. The present work therefore approximates the lumped uncertainty directly by an adaptive fuzzy system rather than identifying individual parameters. The two mechanisms are complementary: identification suits parametric and identifiable uncertainty, whereas approximation suits the non-parametric case.

Although fractional-order PID [17], fractional-order sliding mode control [18], and fuzzy sliding-mode backstepping control for fractional-order systems [19] have been applied to magnetic levitation, these schemes either do not address the uncertain nonlinear function of the MLLSM levitation subsystem or do not combine a differential–integral fractional virtual stabilizing function with online fuzzy approximation.

On the basis of the preceding analysis and related studies, this study designs an adaptive fuzzy fractional-order backstepping control (AFFOBC) to overcome the effects of uncertainty factors including parameter variations and external disturbances within the MLLSM suspension system. First, an FOBC scheme is developed by extending the traditional BC to enhance the tracking accuracy and dynamic response of the MLLSM suspension system. Second, to further strengthen the disturbance rejection ability of the magnetic levitation platform, a fuzzy approximator is adopted for real-time estimation of the uncertain nonlinear functions present in the system, and an adaptive law is designed to achieve adaptive adjustment of control parameters. The estimated values are incorporated into the controller to design an AFFOBC. Finally, through simulation and experimental analysis, it is verified that the control system can still ensure stability and rapid response even when subjected to uncertainties.

The novelty of the proposed AFFOBC lies in three aspects. First, the fractional-order virtual stabilizing function (16) contains independent differential and integral orders a and b, whereas existing schemes use a single order or an integer-order function. Second, the fuzzy system approximates the lumped uncertainty $\Delta f(z)$ arising from feedback linearization of subsystem (12), so the approximation is tied to the linearization residual rather than to a generic unknown nonlinearity. Third, the compensation u_s,sgn(e_3) with $u_s \geq \omega max$ renders $\dot{V}A \leq 0$ for both signs of e_3, which the constant-offset formulation does not.

2. Mathematical Model of MLLSM

The d-q axis voltage equation of the MLLSM is expressed as follows [21]:

$$\begin{cases} u_d = r_s i_d + \dfrac{d\psi_d}{dt} - \dfrac{\pi}{\tau} v \psi_q \\ u_q = r_s i_q + \dfrac{d\psi_q}{dt} + \dfrac{\pi}{\tau} v \psi_d \\ u_f = r_f i_f + \dfrac{d\psi_f}{dt} \end{cases} \tag{1}$$

In the above equations, u_d and u_q denote the direct-axis and quadrature-axis voltages of the armature winding, respectively; u_f represents the excitation winding voltage; ψ_d and ψ_q correspond to the direct-axis and quadrature-axis flux linkages of the armature winding, respectively; ψ_f stands for the excitation flux linkage; i_d and i_q are the direct-axis and quadrature-axis currents of the armature winding, respectively; i_f is the field winding current; r_s and r_f represent the resistances of the armature winding and the excitation winding, respectively; v denotes the linear motor speed; τ is the pole pitch; f is the supply frequency, $v = 2f\tau$.

The flux-linkage equations are expressed as:

$$\begin{cases} \psi_d = i_d L_{md} + i_d L_\sigma + i_f L_{md} \\ \psi_q = i_q L_{mq} + i_q L_\sigma \\ \psi_f = i_f L_{md} + i_f L_{\sigma f} + i_d L_{md} \end{cases} \tag{2}$$

L_{mq} denotes the quadrature-axis armature reaction inductance, L_σ represents the armature winding leakage inductance, and $L_{f\sigma}$ stands for the excitation winding leakage inductance.

Using vector control with $i_d = 0$, the suspension force equation can be obtained as [16]:

$$F_y = \frac{3}{2}[i_f^2 \frac{\partial L_{md}}{\partial \delta} + i_q^2 \frac{\partial L_{mq}}{\partial \delta}] \tag{3}$$

where δ denotes the suspension height at which the moving platform is levitated. The first term of Equation (3) is the levitation force produced by the excitation current. The second term is an additional vertical attraction produced by the armature current, because the q-axis magnetizing inductance L_{mq} also decreases as the air gap increases, so that the armature current required to generate thrust inevitably contributes a normal force proportional to i_q^2. This term is always attractive, is bounded, the armature current is limited by the rated current and $\partial L_{mq}/\partial \delta$ is finite over the operating range, and it varies with the thrust command; its effect is therefore a bounded, operating-point-dependent bias of the levitation force. Because $\partial L_{mq}/\partial \delta$ depends on the operating point and cannot be obtained accurately online, the term is not compensated separately but is lumped with the other uncertainties into f in Equation (5), where it is reconstructed by the adaptive fuzzy approximator together with the robust compensation term. Treating it as a perturbation is thus a modeling choice that keeps the term within the estimated uncertainty rather than a neglect of it. Equation (3) can be rewritten as:

$$F_y = \frac{3}{2} i_f^2 \frac{\partial L_{md}}{\partial \delta} = K(\frac{i_f}{\delta})^2 \tag{4}$$

where: K is the magnetic levitation coefficient, $K = 5.569 \times 10^{-6}$.

The vertical motion equation is expressed as follows:

$$m\frac{\mathrm{d}^2\delta}{\mathrm{d}t^2} = F_y - mg - f \tag{5}$$

Here, m is the moving platform mass and f is the uncertain disturbance, which collects the armature attraction term of Equation (3) together with the other unmodeled effects and external disturbances.

Figure 1 labels the excitation winding and the stator core, the armature winding and the mover core, and the motion platform and auxiliary guide rail. A DC current is injected into the excitation winding housed in the stator core, producing a constant excitation field in the air gap. The mover core is attracted by this field in the vertical direction, generating the levitation force; stable levitation is achieved when this attraction balances the platform weight. A three-phase symmetrical AC current is injected into the armature winding housed in the mover core, producing a traveling field whose interaction with the excitation field generates the horizontal thrust that drives the platform along the guide rail.

Taking state variables $x_1 = \delta$, $x_2 = \dot{\delta}$, $x_3 = i_f$ and output $y = x_1$, the state equation of the MLLSM levitation system can be expressed as:

$$\begin{cases} f(\boldsymbol{x}) = \begin{bmatrix} x_2 \\ \dfrac{Kx_3^2}{mx_1^2} - g - \dfrac{1}{m}f \\ \dfrac{x_3 x_2}{x_1} - \dfrac{3r_f x_3 x_1}{2K} \end{bmatrix}, g(\boldsymbol{x}) = \begin{bmatrix} 0 \\ 0 \\ \dfrac{3x_1}{2K} \end{bmatrix} \\ \dot{\boldsymbol{x}} = f(\boldsymbol{x}) + g(\boldsymbol{x})u \\ y = h(\boldsymbol{x}) = x \end{cases} \tag{6}$$

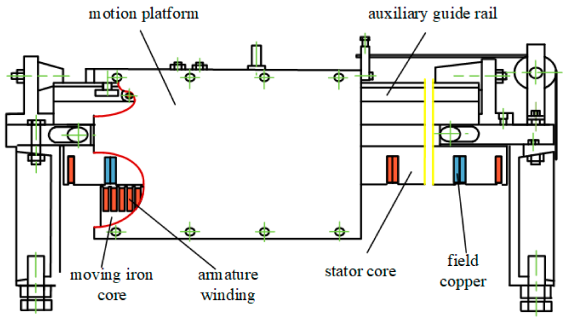


Figure 1. Schematic diagram of the motor's electromagnetic structure.

3. Adaptive Fuzzy Fractional-Order Backstepping Control System Design for MLLSM Levitation System

3.1. Feedback Linearization of MLLSM Levitation System

Equation (6) reveals that the MLLSM levitation system does not satisfy the strict-feedback form and exhibits significant nonlinearity; therefore, feedback linearization (FL) is employed to transform the nonlinear levitation system into a linear one through coordinate transformation and state feedback [25]. To determine whether feedback linearization may be applied, the Lie derivative operation is performed on Equation (6), and the following results are obtained:

$$\begin{aligned} L_g h(\boldsymbol{x}) &= \frac{\partial h(\boldsymbol{x})}{\partial \boldsymbol{x}} g(\boldsymbol{x}) = 0 \\ L_g L_f h(\boldsymbol{x}) &= \frac{\partial L_f h(\boldsymbol{x})}{\partial \boldsymbol{x}} g(\boldsymbol{x}) = 0 \\ L_g L_f^2 h(\boldsymbol{x}) &= \frac{\partial L_f^2 h(\boldsymbol{x})}{\partial \boldsymbol{x}} g(\boldsymbol{x}) = \frac{3x_3}{mx_1} \neq 0 \end{aligned} \tag{7}$$

where L represents the Lie derivative, $L_g h(\boldsymbol{x})$, $L_g L_f h(\boldsymbol{x})$ are the Lie derivative of $h(\boldsymbol{x})$ and $L_f h(\boldsymbol{x})$ along the vector field $g(\boldsymbol{x})$, and $L_f^2 h(\boldsymbol{x})$ is the Lie derivative of order 2 of $h(\boldsymbol{x})$ to $f(\boldsymbol{x})$. Equation (7) indicates that the relative order of the system is 3, which matches the dimension of system (6); hence, feedback linearization of the levitation system is feasible.

According to the definition of relative order and the theory of feedback linearization, the Lie derivative of the corresponding relative order is taken for the output function, and the feedback law is given by

$$u = \alpha(\boldsymbol{x}) + \beta(\boldsymbol{x})u' \tag{8}$$

In the above, u' represents the new control input; $\alpha(\boldsymbol{x})$ and $\beta(\boldsymbol{x})$ are

$$\alpha(\boldsymbol{x}) = -\frac{L_f^3 h(\boldsymbol{x})}{L_g L_f^2 h(\boldsymbol{x})} = r_f x_3 \tag{9}$$

$$\beta(\boldsymbol{x}) = \frac{1}{L_g L_f^2 h(\boldsymbol{x})} = \frac{mx_1}{3x_3} \tag{10}$$

Here, $L_f^3 h(\boldsymbol{x})$ denotes the third-order Lie derivative of $h(\boldsymbol{x})$ with respect to $f(\boldsymbol{x})$. Selection of the nonlinear coordinate map:

$$\boldsymbol{Z} = \begin{bmatrix} h(\boldsymbol{x}) \\ L_f h(\boldsymbol{x}) \\ L_f^2 h(\boldsymbol{x}) \end{bmatrix} = \begin{bmatrix} x_1 \\ x_2 \\ \dfrac{K x_3^2}{m x_1^2} - g - \dfrac{1}{m} f \end{bmatrix} \tag{11}$$

The linear system equations for the state variable $\boldsymbol{Z}$ are

$$\begin{cases} \dot{z}_1 = z_2 \\ \dot{z}_2 = z_3 \\ \dot{z}_3 = f(\boldsymbol{z}) + g(\boldsymbol{z}) u \\ f(z) = f_1(z) + \Delta f(z),\ g(z) = \dfrac{3x_3}{m x_1},\ f_1(z) = -\dfrac{3x_3^2 r_f}{m x_1} \end{cases} \tag{12}$$

where $\Delta f(\boldsymbol{z})$ is the uncertain unknown function generated by the perturbation f_y, and z_1, z_2, and z_3 are the new state variables obtained after the feedback linearization and all of them have real physical significance, which denote the height of the air gap, the velocity, and the acceleration, respectively, of the MLLSM levitation system. Using the nonlinear coordinate mapping relationship of Equation (11), a controller can be designed for the system (12) to achieve control of the nonlinear system.

3.2. Fractional-Order Backstepping Controller Design

Although conventional backstepping control can realize position tracking of the system, optimal performance is often difficult to achieve in practical applications. To improve the transient and steady-state responses of the MLLSM levitation system, fractional-order theory is introduced into the backstepping design to construct a fractional-order virtual stabilizing function, thereby broadening the adjustable range of controller parameters.

The fractional-order differential integral operator ${}_{t_0}D_t^{\lambda}$ is denoted as

$${}_{t_0}D_t^{\lambda} = \begin{cases} \dfrac{\mathrm{d}^{\lambda}}{\mathrm{d}t^{\lambda}}, & \lambda > 0 \\ 1, & \lambda = 0 \\ \int_{t_0}^{t} (\mathrm{d}\tau)^{-\lambda}, & \lambda < 0 \end{cases} \tag{13}$$

where t_0 is the initial condition, and λ represents the order [26]. For ease of notation, in this paper, the fractional-order operator ${}_{t_0}D_t^{\lambda}$ is denoted as D^{λ}. The steps for designing the fractional-order backstepping controller are as follows.

Step 1: The position tracking error is defined as e_1.

$$e_1 = z_{1d} - z_1 \tag{14}$$

where z_1 is the actual suspension height, and z_{1d} is the reference suspension height.

Derivation of Equation (14)

$$\dot{e}_1 = \dot{z}_{1d} - z_2 \tag{15}$$

Construct the fractional-order virtual stability function α as

$$\alpha = \dot{z}_{1d} + k_1 e_1 + c_1 D^a e_1 + c_2 D^{-b} e_1 \tag{16}$$

where a is a fractional-order differential order, b is a fractional-order integral order, and k_1, c_1, c_2 are non-zero positive numbers.

Construct the Lyapunov function $V_1 = \dfrac{1}{2} e_1^2$, derive it, and substitute Equation (16) to obtain

$$\dot{V}_1 = -k_1 e_1^2 + e_1 e_2 - e_1 (c_1 D^a e_1 + c_2 D^{-b} e_1) \tag{17}$$

Step 2: Define the virtual tracking error e_2

$$e_2 = \alpha - z_2 \tag{18}$$

Derivation of Equation (18)

$$\begin{aligned} \dot{e}_2 = \; & \ddot{z}_{1d} + k_1\dot{e}_1 + c_1 D^{1+a} e_1 \\ & + c_2 D^{1-b} e_1 - z_3 \\ & = \dot{\alpha} - z_3 \end{aligned} \tag{19}$$

Construct the virtual stability function β

$$\begin{aligned} \beta = \; & k_2 e_2 + e_1 + \ddot{z}_{1d} + k_1\dot{e}_1 \\ & + c_1 D^{1+a} e_1 + c_2 D^{1-b} e_1 \end{aligned} \tag{20}$$

where k_2 is a non-zero positive number.

Construct the Lyapunov function $V_2 = V_1 + \frac{1}{2}e_2^2$ and derive it

$$\begin{aligned} \dot{V}_2 \; & = -k_1 e_1^2 + e_2(e_1 + \dot{e}_2) \\ & - e_1(c_1 D^a e_1 + c_2 D^{-b} e_1) \end{aligned} \tag{21}$$

Step 3: Define the virtual tracking error e_3

$$e_3 = \beta - z_3 \tag{22}$$

Derivation of Equation (22)

$$\dot{e}_3 = \ddot{\alpha} + \dot{e}_1 + k_2\dot{e}_2 - u' + F_d \tag{23}$$

Construct the Lyapunov function $V_3 = V_2 + \frac{1}{2}e_3^2$ and derive it

$$\begin{aligned} \dot{V}_3 \; & = -k_1 e_1^2 - k_2 e_2^2 + e_3(e_2 + \dot{e}_3) \\ & - e_1(c_1 D^a e_1 + c_2 D^{-b} e_1) \end{aligned} \tag{24}$$

Therefore, the fractional-order backstepping control law is formulated as:

$$\begin{aligned} u'_{FB} \; & = \ddot{\alpha} + k_2\dot{e}_2 - e_3^{-1} e_1(c_1 D^a e_1 + c_2 D^{-b} e_1) \\ & + k_3 e_3 + e_2 + \dot{e}_1 + \rho \mathrm{sgn}(e_3) \end{aligned} \tag{25}$$

The control law (25) is defined for $e_3 \neq 0$. Since the convergence of e_3 is asymptotic, $e_3 = 0$ is reached only in the limit, and the term is well defined for all finite time. In the digital implementation, however, e_3 may become numerically very small, so the inverse is evaluated in the regularized form $e_3^{-1} \to e_3/(e_3^2 + \varepsilon^2)$ with a small positive ε. Outside the boundary layer, $|e_3| \gg \varepsilon$; this coincides with e_3^{-1}, and the cancellation in Equation (27) is exact; inside the boundary layer, the control input remains bounded, and the tracking error is confined to a residual set of size $O(\varepsilon)$.

In the above, $\mathrm{sgn}(\cdot)$ represents the sign function with discontinuous characteristics, given by:

$$\mathrm{sgn}(e_3) = \begin{cases} 1, & e_3 > 0 \\ 0, & e_3 = 0 \\ -1, & e_3 < 0 \end{cases} \tag{26}$$

To ensure the stability of the fractional-order backstepping controller, it is necessary to satisfy $\dot{V}_3 \leq 0$. Substitute Equation (25) into Equation (24):

$$\begin{aligned} \dot{V}_3 \; & = -k_1 e_1^2 - k_2 e_2^2 - k_3 e_3^2 - e_3 \rho \mathrm{sgn}(e_3) + e_3 F_d \\ & \leq -k_1 e_1^2 - k_2 e_2^2 - k_3 e_3^2 + |e_3|(-\rho + |F_d|) \\ & \leq -k_1 e_1^2 - k_2 e_2^2 - k_3 e_3^2 \leq 0 \end{aligned} \tag{27}$$

From Equation (27), $\dot{V}_3$ is negative definite, and then the values of e_1, e_2 and e_3 gradually converge to zero, thus confirming the stability of the proposed fractional-order backstepping control system.

4. Design of Adaptive Fuzzy Fractional-Order Backstepping Control System

To further enhance the control accuracy of the MLLSM levitation system, a fuzzy system is used to approximate the uncertain unknown function in the levitation system. The adaptive law design is derived according to Lyapunov's theorem, and the estimated value is introduced into the fractional-order backstepping control. An adaptive fuzzy fractional-order backstepping control system is designed to effectively improve the disturbance rejection capability of the MLLSM levitation system.

The MLLSM levitation system will be affected by uncertainties such as external disturbances and parameter perturbations during the actual operation, so the exact value of $f(z)$ in Equation (11) cannot be obtained. Therefore, $f(z)$ is defined as

$$f(z) = f_1(z) + \Delta f(z) \tag{28}$$

where $f_1(z)$ is a known quantity, and $\Delta f(z)$ is the uncertain unknown function generated by the perturbation. Because of the universal approximation property of fuzzy logic systems, the uncertain unknown function $\Delta f(z)$ is approximated by a fuzzy system $\Delta\hat{f}(z, \boldsymbol{\theta}_{\Delta f})$. The inputs of the fuzzy system are chosen as the state vector $z = (z_1, z_2, z_3)$ of the linearized subsystem (12), i.e., the air-gap height, its rate of change, and its acceleration, because the uncertain function $\Delta f(z)$ originates from the perturbation after feedback linearization and therefore depends on the same state variables; any other choice of regression vector would leave part of the state dependence of $\Delta f(z)$ unmodeled. According to the fuzzy control principle, the fuzzy rule is

$$\begin{aligned} &\mathrm{R}^{(l)}: \text{ IF } z_1 \text{ is } F_1^l \text{ and} \cdots \text{and } z_n \text{ is } F_n^l; \\ &\text{Then } \Delta\hat{f}(z, \boldsymbol{\theta}_{\Delta f}) \text{ is } A^l \end{aligned} \tag{29}$$

where $n = 3$ is the number of fuzzy system inputs, m_i is the number of membership functions for the i-th input, $l = 1, 2, \ldots, M$ is the rule index, and $M = \prod_{i=1}^{n} m_i = 125$ is the total number of fuzzy rules.

The output generated by the adaptive fuzzy system is expressed as obtained by means of a single-valued fuzzifier, product inference, Gaussian membership functions and a center-average defuzzifier as

$$\Delta\hat{f}(z, \boldsymbol{\theta}_{\boldsymbol{\Delta f}}) = \sum_{l=1}^{M} \theta_l \xi_l(z) = \boldsymbol{\theta}_{\boldsymbol{\Delta f}}^{\mathrm{T}} \boldsymbol{\xi}_f(z) \tag{30}$$

where $\theta_{\Delta f} = (\theta_1, \ldots, \theta_M)^{\mathrm{T}}$. θ_l is a control parameter whose initial value is set to 0.01. $\xi_{\Delta f}(z) = (\xi_1(z), \ldots, \xi_{1M}(z))^{\mathrm{T}}$, $\xi_l(z)$ is the fuzzy basis function defined as

$$\xi_l(z) = \frac{\prod_{i=1}^{n} \mu_{F_i^l}(z_i)}{\sum_{l=1}^{M} \prod_{i=1}^{n} \mu_{F_i^l}(z_i)} \tag{31}$$

where $\mu_{F_i^l}(z_i)$ is the Gaussian membership function of the l-th fuzzy set for the i-th input. The reference air-gap height of the MLLSM levitation system is $\sigma_0 = 2.5 \times 10^{-3}$ m, and the membership functions are chosen with centers distributed uniformly across the admissible operating range of each state and with widths set so that adjacent membership functions overlap, thereby satisfying the fuzzy partition condition $\sum_{l=1}^{m_i} \mu_{F_i^l}(z_i) = 1$ required by the basis-function expansion (31). Accordingly, the membership functions are chosen as

$$\begin{aligned}\mu_{F_1^l}(z_1) &= \exp[-(\frac{z_1 - \pi(m-1)/2400}{\pi/4800})^2] \\ \mu_{F_2^l}(z_2) &= \exp[-(\frac{z_2 - \pi(m-3)/120}{\pi/240})^2] \\ \mu_{F_3^l}(z_3) &= \exp[-(\frac{z_3 - \pi(m-3)/2}{\pi/4})^2]\end{aligned} \tag{32}$$

Each input is partitioned into $m_i = 5$ fuzzy sets, giving $M = \prod_{i=1}^{n} m_i = 125$ rules. This value follows the conventional compromise used in fuzzy-approximation designs: the universal approximation property guarantees that the approximation error can be made arbitrarily small by increasing M, while the computational burden grows as m_i^n. Increasing m_i therefore improves the tracking accuracy only until the approximation error falls below the level relevant to the control accuracy, beyond which it adds cost without benefit.

Where $m = 1, \ldots, 5$. The resulting fuzzy system output $\Delta\hat{f}(z, \boldsymbol{\theta}_{\Delta f})$ is introduced into the FOBC. Here, we introduce a compensating control term u_s to ensure the stability of the control system. From this, the adaptive fuzzy fractional-order backstepping control law is obtained as

$$\begin{aligned}u_A = g(z)^{-1}[&\ddot{\alpha} + k_2\dot{e}_2 - e_3^{-1}e_1(c_1D^a e_1 + c_2D^{-b}e_1) + \\ &k_3e_3 + e_2 + \dot{e}_1 - f_1(z) - \Delta\hat{f}(z, \theta_{\Delta f}) - u_s\mathrm{sgn}(e_3)]\end{aligned} \tag{33}$$

In Equation (33), the fuzzy term and the sign-based term play distinct roles: $\Delta\hat{f}(z, \theta\Delta f)$ approximates the unknown function $\Delta f(z)$, model uncertainty, parameter deviation and external disturbance, whereas u_s,$\mathrm{sgn}(e_3)$ compensates only the residual approximation error ω, with $u_s \geq \omega max$ required by Equation (43). Since the fuzzy approximation reduces the magnitude of the uncertainty from $|F_d|$ to ω_{max}, the switching amplitude is correspondingly reduced, without eliminating the robust term itself.

The optimum parameter vector is defined as

$$\boldsymbol{\theta}^*_{\boldsymbol{\Delta f}} = \mathrm{argmin}_{\boldsymbol{\theta}_{\boldsymbol{\Delta f}} \in \Omega_{\Delta f}}[\sup_{z \in R^n}\left|\Delta\hat{f}(z, \boldsymbol{\theta}_{\Delta f}) - \Delta f(z)\right|] \tag{34}$$

where Ω_Δ is the set of constraints on $\boldsymbol{\theta}_{\boldsymbol{\Delta f}}$.

The optimal fuzzy approximation error is defined as

$$\omega = \Delta\hat{f}(z, \boldsymbol{\theta}^*_{\boldsymbol{\Delta f}}) - \Delta f(z) \tag{35}$$

where $|\omega| \leq \omega_{\max}$, and $\omega_{\max}$ is defined as

$$\omega_{\max} = \max_{\boldsymbol{\theta}_{\Delta f} \in \boldsymbol{\Omega}_{\Delta f}, z \in R^n}\left|\Delta\hat{f}(z, \boldsymbol{\theta}_{\Delta f}) - \Delta f(z)\right| \tag{36}$$

Construct the Lyapunov function V_A as

$$V_A = V_3 + \frac{1}{2r_{\Delta f}}\boldsymbol{\varphi}^{\mathrm{T}}_{\boldsymbol{\Delta f}}\boldsymbol{\varphi}_{\boldsymbol{\Delta f}} \tag{37}$$

where $r_{\boldsymbol{\Delta f}}$ is the gain coefficient, taken as a non-zero positive number. $\boldsymbol{\varphi}_{\boldsymbol{\Delta f}}$ is defined in the following form:

$$\boldsymbol{\varphi}_{\boldsymbol{\Delta f}} = \boldsymbol{\theta}^*_{\boldsymbol{\Delta f}} - \boldsymbol{\theta}_{\boldsymbol{\Delta f}} \tag{38}$$

Derivation of Equation (37) yields

$$\begin{aligned}\dot{V}_A &= \dot{V}_3 + \frac{1}{r_{\Delta f}}\boldsymbol{\varphi}^{\mathrm{T}}_{\boldsymbol{\Delta f}}\dot{\boldsymbol{\varphi}}_{\boldsymbol{\Delta f}} \\ &= -k_1e_1^2 - k_2e_2^2 + e_3[e_2 + \dot{e}_3 + e_1 + k_2\dot{e}_2 - f_1(z) - \Delta f(z) - g(z)u_A] \\ &\quad -e_1(c_1D^a e_1 + c_2D^{-b}e_1) + \frac{1}{r_{\Delta f}}\boldsymbol{\varphi}^{\mathrm{T}}_{\boldsymbol{\Delta f}}\dot{\boldsymbol{\varphi}}_{\boldsymbol{\Delta f}}\end{aligned} \tag{39}$$

Substituting Equation (33) into Equation (39) yields

$$\begin{aligned}\dot{V}_A &= -k_1e_1^2 - k_2e_2^2 - k_3e_3^2 + e_3[\boldsymbol{\varphi}_{\boldsymbol{\Delta f}}^{\mathrm{T}}\boldsymbol{\xi}(z) + \omega - u_s] + \frac{1}{r_{\Delta f}}\boldsymbol{\varphi}_{\boldsymbol{\Delta f}}^{\mathrm{T}}\dot{\boldsymbol{\varphi}}_{\boldsymbol{\Delta f}} \\ &= -k_1e_1^2 - k_2e_2^2 - k_3e_3^2 + \frac{1}{r_{\Delta f}}\boldsymbol{\varphi}_{\boldsymbol{\Delta f}}^{\mathrm{T}}[r_{\Delta f}e_3\boldsymbol{\xi}(z) + \dot{\boldsymbol{\varphi}}_{\boldsymbol{\Delta f}}] + e_3(\omega - u_s)\end{aligned} \tag{40}$$

Selected according to Equation (40)

$$r_{\Delta f}e_3\boldsymbol{\xi}(z) + \dot{\boldsymbol{\varphi}}_{\boldsymbol{\Delta f}} = 0 \tag{41}$$

This gives the adaptive law as

$$\dot{\boldsymbol{\theta}}_{\boldsymbol{\Delta f}} = -\dot{\boldsymbol{\varphi}}_{\boldsymbol{\Delta f}} = r_{\Delta f}e_3\boldsymbol{\xi}(z) \tag{42}$$

The adaptive law given in Equation (42) is employed to adjust the fuzzy system parameters online, so as to achieve optimal control performance.

The asymptotic stability of the affine nonlinear system with uncertain unknown functions described by Equation (11) is ensured by the control law (33) together with the adaptive law (42).

Proof. Construct a Lyapunov function $\dot{V}_A$ as shown in Equation (34), and its derivation leads to Equation (40). Substituting the adaptive law in Equation (42) into Equation (40) leads to

$$\begin{aligned}&\dot{V}_A = -k_1e_1^2 - k_2e_2^2 - k_3e_3^2 + e_3(\omega - u_s\mathrm{sgn}(e_3)) \\ &\leq -k_1e_1^2 - k_2e_2^2 - k_3e_3^2 + |e_3|(\omega_{max} - u_s) \leq 0\end{aligned} \tag{43}$$

According to the universal approximation theorem for fuzzy systems, the designed AFC can guarantee that the approximation error $\omega_{\max}$ is a very small value. Let $u_s \geq \omega_{\max}$, then $\dot{V}_A \leq 0$ can be satisfied.

To verify the stability of the proposed control system, define $W(t)$ as

$$W(t) = k_1e_1^2 + k_2e_2^2 + k_3e_3^2 \geq 0, \dot{V}_A \leq -W(t) \tag{44}$$

From this

$$\int_0^t W(\tau)d\tau \leq V_A(0) - V_A(t) \leq V_A(0) < \infty \tag{45}$$

Since $V_A(0)$ is bounded, $\dot{V}_A$ is a monotonic, non-increasing, non-negative function. It is therefore possible to obtain

$$\int_0^t W(\tau)d\tau \leq V_A(0) - V_A(t) \leq V_A(0) < \infty \tag{46}$$

Moreover, since $W(t)$ is also bounded, $W(\tau)$ is uniformly continuous. By applying Barbalat's lemma, it can be concluded that

$$\lim_{t\to\infty} W(t) = 0 \tag{47}$$

It is observed that as time $t \to \infty$, e_1, e_2, e_3 tend to zero over time, thereby guaranteeing the stability of the proposed control system. □

5. Experimental Verification

To verify the effectiveness of the designed AFFOBC, the MLLSM maglev control system is constructed as shown in Figure 2, and experimental analysis is carried out. The AFFOBC method is compared with the FOBC and BC control methods. The AFFOBC parameters are fully tuned to obtain the following values: $r_{\Delta f} = 5 \times 10^5$, $k_1 = 320$, $k_2 = 80$, $k_3 = 55$, $c_1 = 0.3$, $c_2 = 0.2$, $a = 0.4$, $b = 0.3$, $u_s = 2.5$. Motor parameters are shown in

Table 1. The three controllers are compared as a nested design rather than as independently optimized competitors: BC is the integer-order baseline, FOBC adds the fractional-order virtual stabilizing function, and AFFOBC further adds the adaptive fuzzy approximation and the robust compensation term. All controllers were tuned by the same trial-and-error procedure over repeated simulations to achieve the best steady-state and dynamic performance, and they share identical gains wherever the design is common: $k_1 = 320$, $k_2 = 80$, $k_3 = 55$ for all three; $c_1 = 0.3$, $c_2 = 0.2$, $a = 0.4$, $b = 0.3$ for FOBC and AFFOBC; only AFFOBC additionally uses $u_s = 2.5$ and $r_{\Delta f} = 5 \times 10^5$. The comparison therefore isolates the effect of each added design element under otherwise identical tuning conditions. The parameters are listed in Table 2. The step load and the periodic disturbance used in this section are applied as external forces on the levitation subsystem, and therefore enter Equation (5) through the same channel as the armature-attraction term of Equation (3). The tests thus verify the rejection of bounded perturbations of the same class.

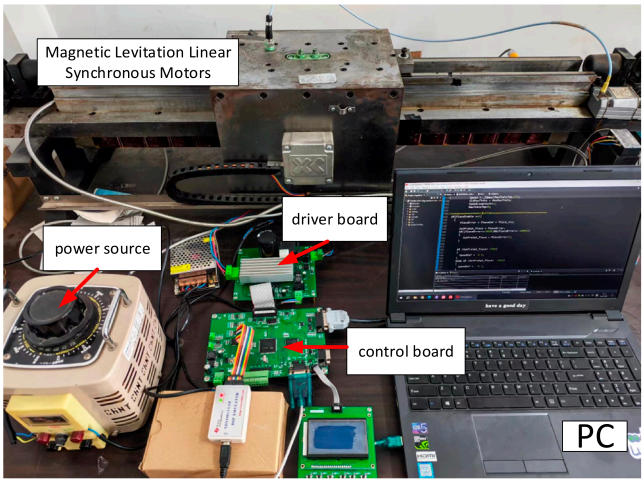


Figure 2. Configuration of the MLLSM Levitation Control System.

Table 1. Motor Parameters.

Parameter	Symbol	Value	Unit
Pole pitch	τ	48	mm
Number of pole pairs	p	3	—
Supply frequency	f	10	Hz
Phase number	—	3	—
Rated current	I_N	2.5	A
Armature winding resistance	R_s	1.2	Ω
Excitation winding resistance	R_f	18	Ω
d-axis inductance	L_d	18	mH
q-axis inductance	L_q	58.98	mH
d-axis armature reaction inductance	L_md	9.5	mH
Turns per phase	N	600	—
Mover/load mass	M	10	kg
Rated speed	V	0.96	m/s
Reference air gap	δ_0	2.5	mm

Table 2. Controller Parameter Table.

Controller	k_1	k_2	k_3	c_1	c_2	a	b	u_s	$r_{\Delta f}$
BC	320	80	55	—	—	—	—	—	—
FOBC	320	80	55	0.3	0.2	0.4	0.3	—	—
AFFOBC	320	80	55	0.3	0.2	0.4	0.3	2.5	5×10^5

(1) The startup performance of the MLLSM levitation system is examined. A reference suspension height of 2.5 mm is adopted. Figure 3 illustrates the suspension height response of the levitation system, and Figure 4 presents the corresponding suspension height error.

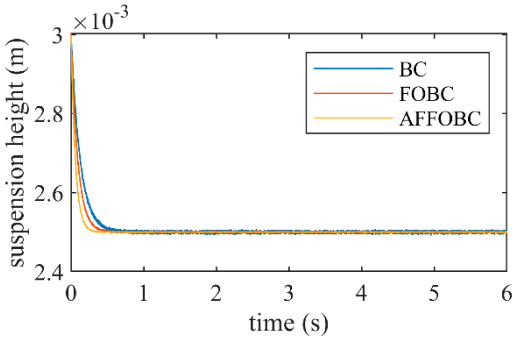


Figure 3. Suspension height response curve at startup.

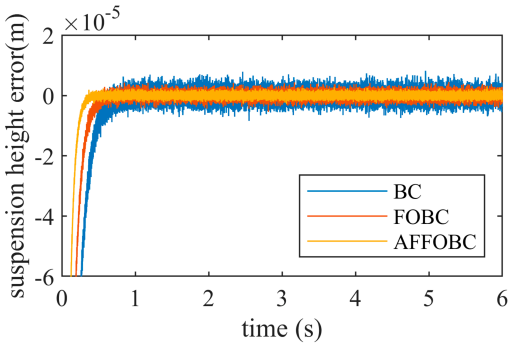


Figure 4. Suspension height error curve at start-up.

During startup of the MLLSM levitation system, no overshoot is observed in any of the three control methods. Using AFFOBC control, the time required for the levitation system's suspension height to reach the set value is 0.32 s, which is 37.3% and 59.5% faster than the 0.51 s and 0.79 s achieved by FOBC control and BC control, respectively. This indicates that the AFFOBC control method exhibits faster response speeds during both the rise and regulation processes, thereby enhancing the system's overall response speed to a certain extent.

(2) Analyze the interference-resistance performance of the MLLSM levitation system when subjected to sudden load disturbances. The load disturbance signal is applied at 2 s and removed at 4 s. Figure 5 presents the suspension height response of the levitation system, while Figure 6 shows the corresponding suspension height error.

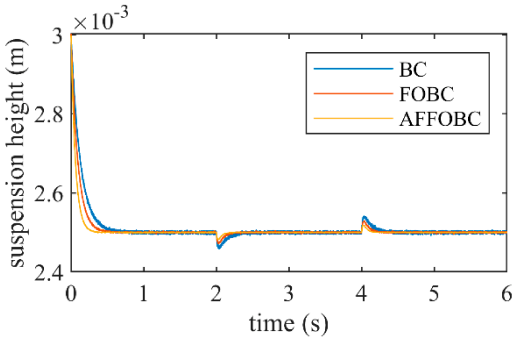


Figure 5. Suspension height response curve under sudden load disturbance.

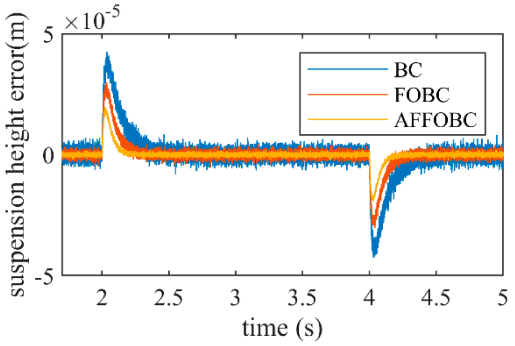


Figure 6. Suspension height error curve during sudden load disturbance.

As shown in Figure 6, when the MLLSM levitation system is subjected to sudden load disturbances, using AFFOBC control results in minimal fluctuations in the system's suspension height, with a maximum dynamic error of approximately 1.9×10^{-5} m, which is 32.1% and 51.3% lower than the 2.8×10^{-5} m and 3.9×10^{-5} m achieved by FOBC control and BC control, respectively. The recovery time for AFFOBC control is 0.23 s, which is 23.3% and 53.1% shorter than the 0.30 s and 0.49 s achieved by FOBC and BC, respectively. For consistency, the recovery time is defined as the interval from load removal ($t = 4$ s) until the air-gap error re-enters and stays within a band of ±2% of the reference height ($\pm 5 \times 10^{-5}$ m); the same band is used for all three controllers. In summary, AFFOBC control effectively reduces suspension height fluctuations under a periodic sinusoidal disturbance and rapidly restores the air gap to the reference height when subjected to sudden load disturbances, demonstrating excellent interference-resistance performance.

As shown in Figure 6, the suspension height fluctuation under AFFOBC is the smallest among the three controllers. The fuzzy approximator estimates the unknown lumped function online; therefore, the uncertainty that the switching term has to cover is reduced from the full disturbance to the small residual approximation error. The amplitude of the switching term is therefore much smaller in AFFOBC than in BC and FOBC, which reduces the high-frequency control activity and the resulting air-gap fluctuation. We note, however, that the present data characterize the air-gap response only; a direct comparison of the control inputs and a dedicated chattering measure are left to future work.

The excitation-current records are shown in Figure 7. The current ripple is approximately 3×10^{-3} A under BC and 1.5×10^{-3} A under FOBC, whereas under AFFOBC it is no longer discernible.

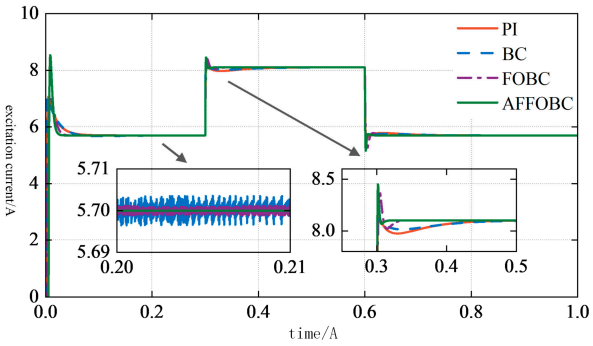


Figure 7. Excitation current response curve during sudden load disturbance.

(3) The suppression performance of the MLLSM levitation system against periodic sinusoidal disturbance is investigated. Periodic sinusoidal disturbances are emulated by injecting a sinusoidal disturbance $fy = 15sin(2\pi t)N$ for a duration of 3 s. The resulting

suspension height response and the corresponding tracking error are presented in Figure 8 and Figure 9, respectively.

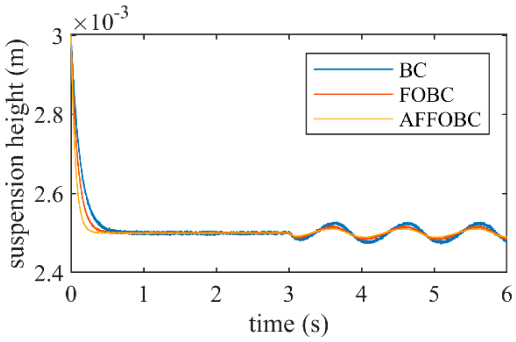


Figure 8. Suspension height response curve under sudden sinusoidal disturbance.

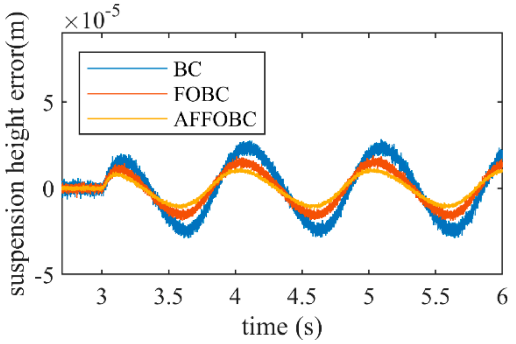


Figure 9. Suspension height error curve under sudden sinusoidal disturbance.

As shown in Figures 8 and 9, when using BC control, the system is significantly affected by periodic sinusoidal disturbance, with a maximum dynamic error of 2.8×10^{-5} m; when using FOBC control, the system has a dynamic drop of 1.9×10^{-5} m, demonstrating a significant improvement in interference resistance compared to the BC control system; When using AFFOBC control, the system dynamic descent is 1.1×10^{-5} m, with the smallest suspension height variation and stronger sinusoidal disturbance rejection capability than BC control and FOBC control. In summary, AFFOBC control effectively reduces suspension height fluctuations when affected by periodic sinusoidal disturbance and has strong sinusoidal disturbance rejection capability.

6. Conclusions

For the MLLSM suspension system, an AFFOBC method is proposed, yielding the following conclusions:

(1) The operational mechanism of the MLLSM suspension system is investigated. Using a vector control method with $i_d = 0$, a mathematical model of the MLLSM suspension system is developed, and its state-space equations are derived. Through input–output feedback linearization, the MLLSM suspension system is converted into a linear system.

(2) The AFFOBC method is proposed. A fractional-order virtual stability function is constructed, incorporating differential and integral order terms into the virtual stability function. A FOBC is designed to broaden the adjustable range of controller parameters, thereby significantly improving the transient and steady-state responses of the suspension system. To further enhance the control performance of the MLLSM suspension system, an adaptive fuzzy system is developed to approximate the uncertain unknown functions within it; a Lyapunov function is constructed to prove system stability.

(3) Perform experimental research on the suspension control system. Compare the AFFOBC with conventional BC and FOBC. Experimental results confirm that the AFFOBC enhances the dynamic response of the suspension system and effectively attenuates the influence of uncertain disturbances on it.

Author Contributions: Conceptualization, Y.S. and T.F.; methodology, Y.S. and T.F.; software, T.F. and W.B.; validation, T.F., Y.Z. and L.X.; formal analysis, T.F.; investigation, Y.Z. and L.X.; resources, Y.Z.; data curation, W.B.; writing—original draft preparation, T.F.; writing—review and editing, Y.S.; visualization, W.B. and L.X.; supervision, Y.S.; project administration, Y.S.; funding acquisition, Y.S. All authors have read and agreed to the published version of the manuscript.

Funding: This work was supported by the Basic Scientific Research Project of Colleges and Universities in Liaoning Province under Grant LJ212411632065 and the Joint Program of Liaoning Provincial Science and Technology Plan (Natural Science Foundation—Doctoral Scientific Research Startup Project) under Grant No. 2024-BSLH-158.

Data Availability Statement: The original contributions presented in this study are included in the article. Further inquiries can be directed to the corresponding author.

Conflicts of Interest: Author Yu Zhang was employed by the company Panshan County Power Supply Company, State Grid Liaoning Panjin Power Supply Company. The remaining authors declare that the research was conducted in the absence of any commercial or financial relationships that could be construed as a potential conflict of interest.

References

1. Wang, X.; Zhong, Z.; Wang, Y.; Jiang, B.; Chen, W. Magnetic Levitation Control of Doubly Fed Linear Motor With Multiphase AC Excited Mover. *IEEE J. Emerg. Sel. Top. Power Electron.* **2025**, *13*, 2590–2600. [CrossRef]
2. Meng, B.; Li, M.; Liu, X.; Wang, L.; Liang, S.Y.; Wang, Z. Research progress on the architecture and key technologies of machine tool intelligent control system. *J. Mech. Eng.* **2021**, *57*, 147–166. [CrossRef]
3. Shi, H.; Yang, W.; Fu, S.; Liu, H.; Yang, J.; Li, K.; Deng, Z. Characteristics Analysis and Dynamic Test of Air-Cored Permanent Magnet Linear Synchronous Motor for Null-Flux PMEDS Vehicle. *IEEE Trans. Instrum. Meas.* **2024**, *73*, 1–15. [CrossRef]
4. Zhao, C.; Sun, F.; Jin, J.; Pei, W.; Xu, F.; Oka, K.; Zhang, M. Research of permanent levitation system: Analysis, control strategy design, and experiment. *Proc. Inst. Mech. Eng. Part C J. Mech. Eng. Sci.* **2022**, *236*, 7617–7628. [CrossRef]
5. Wang, M.; Hao, Z.; He, Y.; Zeng, S.; Qi, Z.; Liu, P. Active disturbance rejection backstepping cross-coupling controller design for a magnetic levitation vehicle suspension frame. *IEEE Trans. Transp. Electrif.* **2025**, *11*, 4634–4644. [CrossRef]
6. Fattah, R.; Kenné, J.-P.; Benjelloun, K.; Chebak, A. Optimization of the backstepping control parameters of an active electrohydraulic suspension to improve passenger comfort and road handling. *IEEE Access* **2025**, *13*, 35985–36005. [CrossRef]
7. Siffat, S.A.; Ahmad, I.; Rahman, A.U.; Islam, Y. Robust integral backstepping control for unified model of hybrid electric vehicles. *IEEE Access* **2020**, *8*, 49038–49052. [CrossRef]
8. Wang, J.; Alattas, K.A.; Bouteraa, Y.; Mofid, O.; Mobayen, S. Adaptive finite-time backstepping control tracker for quadrotor UAV with model uncertainty and external disturbance. *Aerosp. Sci. Technol.* **2023**, *133*, 108088. [CrossRef]
9. Xie, W.; Cabecinhas, D.; Cunha, R.; Silvestre, C. Adaptive backstepping control of a quadcopter with uncertain vehicle mass, moment of inertia, and disturbances. *IEEE Trans. Ind. Electron.* **2021**, *69*, 549–559. [CrossRef]
10. Yu, D.; Ma, S.; Liu, Y.-J.; Wang, Z.; Chen, C.L.P. Finite-time adaptive fuzzy backstepping control for quadrotor UAV with stochastic disturbance. *IEEE Trans. Autom. Sci. Eng.* **2023**, *21*, 1335–1345. [CrossRef]
11. Zheng, K.; Zhang, Q.; Hu, Y.; Wu, B. Design of fuzzy system-fuzzy neural network-backstepping control for complex robot system. *Inf. Sci.* **2021**, *546*, 1230–1255. [CrossRef]
12. Lin, F.-J.; Teng, L.-T.; Shieh, P.-H. Intelligent adaptive backstepping control system for magnetic levitation apparatus. *IEEE Trans. Magn.* **2007**, *43*, 2009–2018. [CrossRef]
13. Adil, H.M.M.; Ahmed, S.; Ahmad, I. Control of MagLev system using supertwisting and integral backstepping sliding mode algorithm. *IEEE Access* **2020**, *8*, 51352–51362. [CrossRef]
14. Fatemimoghadam, A.; Toshani, H.; Manthouri, M. Control of levitation system using recurrent neural network-based adaptive optimal backstepping strategy. *Trans. Inst. Meas. Control* **2020**, *42*, 2382–2395. [CrossRef]
15. Liu, J.; Liu, Y.; Chi, R. Adaptive backstepping iteration learning control of nonlinear feedback systems. *Sci. China Technol. Sci.* **2025**, *68*, 265–266. [CrossRef]

16. Guo, Q.; Zhang, Y.; Celler, B.G.; Su, S.W. Neural adaptive backstepping control of a robotic manipulator with prescribed performance constraint. *IEEE Trans. Neural Netw. Learn. Syst.* **2019**, *30*, 3572–3583. [CrossRef] [PubMed]
17. Cui, H. Application of PID Controller Parameter Optimization Based on Particle Swarm Optimization Algorithm in Position AC Servo System. *Electr. Mot. Technol.* **2026**, 13–16. Available online: https://kns.cnki.net/kcms2/article/abstract?v=txIpKU2KNMoyyboyETW55wnVOfPojYaM-7xHYaVH7wiXL69Jr47K6thtUiv-YU1jbPshM6IagsaEXxlX5eVoHx4PuIZb0ig91tgbdd4KV5pOITQRS3A6xbcqdQSoo6Jlt1E7UTAur9Sd2J3zagRHouNSi9Ka6fX23cxipGJ49d0=&uniplatform=NZKPT (accessed on 1 September 2026).
18. Pandey, S.; Dourla, V.; Dwivedi, P.; Junghare, A. Introduction and realization of four fractional-order sliding mode controllers for nonlinear open-loop unstable system: A magnetic levitation study case. *Nonlinear Dyn.* **2019**, *98*, 601–621. [CrossRef]
19. Li, X.; Wen, C.; Li, X.; He, J. Adaptive fractional-order backstepping control for a general class of nonlinear uncertain integer-order systems. *IEEE Trans. Ind. Electron.* **2023**, *70*, 7246–7256. [CrossRef]
20. Zhao, X.; Wang, L. Finite-time control of permanent magnet linear synchronous motor via variable gain fractional-order terminal sliding mode control. *IEEE Trans. Transp. Electrif.* **2025**, *11*, 9105–9120. [CrossRef]
21. Liu, Y.-C.; Laghrouche, S.; Depernet, D.; Djerdir, A.; Cirrincione, M. Disturbance-observer-based complementary sliding-mode speed control for PMSM drives: A super-twisting sliding-mode observer-based approach. *IEEE J. Emerg. Sel. Top. Power Electron.* **2021**, *9*, 5416–5428. [CrossRef]
22. Wai, R.-J.; Yao, J.-X.; Lee, J.-D. Backstepping fuzzy-neural-network control design for hybrid maglev transportation system. *IEEE Trans. Neural Netw. Learn. Syst.* **2015**, *26*, 302–317. [CrossRef] [PubMed]
23. Yang, C.; Liu, W.; Song, B.; Chau, K.T. Signal-Injection-Free Online Identification of Temperature-Dependent Electrical Parameters for SPMSM Drives: An Alternating Dual-Adaline Approach. *IEEE Trans. Transp. Electrif.* **2026**, *12*, 8447–8463.
24. Zhou, R.; Wang, H. Model Predictive Speed and Voltage Control of Sensorless PMSM with Parameter Rectification and A Reduced-Order EKF. *IEEE Trans. Ind. Electron.* **2026**, 1–13. [CrossRef]
25. Accetta, A.; Cirrincione, M.; D'Ippolito, F.; Pucci, M.; Sferlazza, A. Input–output feedback linearization control of a linear induction motor taking into consideration its dynamic end-effects and iron losses. *IEEE Trans. Ind. Appl.* **2022**, *58*, 3664–3673. [CrossRef]
26. Zhong, C.Q.; Wang, L.; Xu, C.F. Path tracking of permanent magnet synchronous motor using fractional-order fuzzy PID controller. *Symmetry* **2021**, *13*, 1118. [CrossRef]

Disclaimer/Publisher's Note: The statements, opinions and data contained in all publications are solely those of the individual author(s) and contributor(s) and not of MDPI and/or the editor(s). MDPI and/or the editor(s) disclaim responsibility for any injury to people or property resulting from any ideas, methods, instructions or products referred to in the content.